Physics AUC, vol. 17 (part I), 86-99 (2007) PHYSICS AUC

Bounded tokamap

V.N. Kuzovkov

Institute of Solid State Physics, Association Euratom-University of Latvia,

8 Kengaraga Street, LV – 1063 RIGA, Latvia*

O. Dumbrajs

Institute of Solid State Physics, Association Euratom-University of Latvia,

8 Kengaraga Street, LV – 1063 RIGA, Latvia

Abstract

A Hamiltonian map is constructed in which both the polar axis and the boundary of the plasma cannot be crossed upon iteration. Phase portraits of the new map are quite different comparing with tokamap phase portraits. In particular, the Golden KAM exists up to $K \approx 4$ in contrast to tokamap where the Golden KAM plays no special role. It is found that differences in the predictions of the tokamap and bounded tokamap might become significant in those cases when processes at plasma periphery are studied.

1 Introduction

Magnetic field lines in plasmas can be regarded as trajectories of Hamiltonian systems. For the field line tracing two methods can be applied: i) integration of the trajectory and ii) mapping of the trajectory. The latter is a modern technique for the Hamiltonian system. It is more than an order of magnitude faster than the integration. A properly chosen mapping procedure always conserves the main flux preserving property of the magnetic field, which is important for a correct reproduction of the long-term behaviour of field lines in stochastic regions.

Symplectic maps for many Hamiltonian problems have been extensively used during the last four decades. A systematic theory of these maps with many illustrative examples can be found in the recent book [1].

In this work we address a specific question: what are the consequences of the physical condition that the boundary of the plasma cannot be crossed. To answer this question, we reexamine the so called tokamap [2, 3, 4].

The paper is organized as follows. A short description of the tokamap is given in Sec. II. In Sec. III we introduce the physical bound on the magnetic flux and derive the so called bounded tokamap. In Sec. IV we compare phase portraits and KAM barriers of the tokamap and the bounded tokamap. Appendix is devoted to the calculation of fixed points and their stable and unstable manifolds of the bounded tokamap. Finally, a summary and the conclusions are presented in Sec. V.

*E-mail address: kuzovkov@latnet.lv

2 The Tokamap

Mappings are constructed as iterative symplectic maps, representing a global picture of a tokamak cross section at the toroidal angle $\varphi_k = 2\pi k \pmod{2\pi}$. The generating function of the mapping is defined as follows:

$$\delta F\left(\psi_{k+1}, \theta_k\right) = -\frac{K}{\left(2\pi\right)^2} h\left(\psi_{k+1}\right) \cos 2\pi\theta_k \tag{1}$$

and the mapping itself is given by the expressions

$$\begin{aligned} \psi_k &= \psi_{k+1} + \frac{\partial \delta F\left(\psi_{k+1}, \theta_k\right)}{\partial \theta_k} = \\ &= \psi_{k+1} + \frac{K}{2\pi} h\left(\psi_{k+1}\right) \sin\left(2\pi\theta_k\right), \end{aligned} \tag{2}$$

$$\begin{aligned} \theta_{k+1} &= \theta_k + W\left(\psi_{k+1}\right) + \frac{\partial \delta F\left(\psi_{k+1}, \theta_k\right)}{\partial \psi_{k+1}} = \\ &= \theta_k + W\left(\psi_{k+1}\right) - \frac{K}{\left(2\pi\right)^2} h'\left(\psi_{k+1}\right) \cos\left(2\pi\theta_k\right). \end{aligned} \tag{3}$$

Here ψ is the magnetic flux, θ is the poloidal angle, and W is the winding number; its inverse $q = 1/W$ is called the safety factor. The real, positive parameter$K$ is called the stochasticity parameter. It measures the strength of the perturbation.

Choice of the function $h\left(\psi\right)$ in the form

$$h\left(\psi\right) = \frac{\psi}{1+\psi} \tag{4}$$

yields the following map:

$$\psi_{k+1} = \psi_k - \frac{K}{2\pi} \frac{\psi_{k+1}}{1+\psi_{k+1}} \sin 2\pi\theta_k, \tag{5}$$

$$\theta_{k+1} = \theta_k + W\left(\psi_{k+1}\right) - \frac{K}{\left(2\pi\right)^2} \frac{1}{\left(1+\psi_{k+1}\right)^2} \cos 2\pi\theta_k. \tag{6}$$

The specific form of the map (5) and (6) is known as the *tokamap*. It is compatible with the toroidal geometry and describes the global behavior of magnetic field lines in tokamaks.

In form (5), the map is nonlinear; it possesses two solutions ψ_{k+1} for given(ψ_k, θ_k). The following choice of the unique root provides the final definition of the tokamap:

$$\psi_{k+1} = \frac{1}{2}\left\{P\left(\psi_k, \theta_k\right) + \sqrt{\left[P\left(\psi_k, \theta_k\right)\right]^2 + 4\psi_k}\right\}, \tag{7}$$

where the function $P\left(\psi, \theta\right)$ is defined as

$$P\left(\psi, \theta\right) = \psi - 1 - \frac{K}{2\pi} \sin 2\pi\theta. \tag{8}$$

It is easily checked that in this mapping the magnetic flux is a definite positive number. If $\psi_0 > 0$ then $\psi_k > 0$, i.e.

$$\psi \geq 0. \tag{9}$$

It should be noted that Eq. (8) violates the global invariance ($\psi_k = 0 \quad \Rightarrow \quad \psi_{k+1} = 0$) if $\frac{K}{2\pi} \sin(2\pi\theta_k) < -1$. As a consequence in the tokamap *global chaos* appears for $K/2\pi > 1$.

The upper limit

$$\psi \leq 1, \tag{10}$$

which means that plasma boundary cannot be crossed, is not imposed. For this reason the tokamap can be directly used in the ergodic divertor problem [5] where magnetic field lines may go outside the last magnetic surface ($\psi = 1$).

Properties of the tokamap and of its various modifications have been studied in detail [1, 2, 3, 4]. Several applications, e.g., investigation of magnetic reconnection during the crash stage of the sawtooth instability [6] and stochastic transport of magnetic field lines [7] are known.

The question arises what are the consequences of condition (10), should it be imposed into a mapping in those cases when the physical problem is such that the physical bound really exists, e.g., is given by a limiter or the wall?

3 The bounded tokamap

It is rather obvious that the important property of the tokamap Eq. (9) ("the polar axis cannot be crossed"[2]) is related to the boundary condition $h(0) = 0$ following from Eq.(4). By analogy the limit (10) requires another boundary condition $h(1) = 0$. The two conditions can be simultaneously satisfied if instead of Eq.(4) we take the function $h(\psi)$ e.g., in the following form

$$h(\psi) = \psi(1 - \psi). \tag{11}$$

Such a choice yields the following map:

$$\psi_k = \psi_{k+1} + \frac{K}{2\pi}\psi_{k+1}(1 - \psi_{k+1}) \sin(2\pi\theta_k), \tag{12}$$

$$\theta_{k+1} = \theta_k + W(\psi_{k+1}) - \frac{K}{(2\pi)^2}(1 - 2\psi_{k+1}) \cos(2\pi\theta_k). \tag{13}$$

In form (12), the map is nonlinear. We rewrite it in the following form:

$$\psi_k = \psi_{k+1} + Dh(\psi_{k+1}), \tag{14}$$

where

$$D = \frac{K}{2\pi} \sin(2\pi\theta_k) \tag{15}$$

In order to consider a continuous map valid on the polar axis $\psi = 0$, the wall $\psi = 1$ and in the region $0 < \psi < 1$ we choose in (14) the root

$$\psi_{k+1} = \frac{1 + D - \sqrt{(1 + D)^2 - 4D\psi_k}}{2D}. \tag{16}$$

It can be easily checked that the global invariance ($\psi_k = 0 \quad \Rightarrow \quad \psi_{k+1} = 0$ and $\psi_k = 1 \quad \Rightarrow \quad \psi_{k+1} = 1$) holds if $K/2\pi < 1$.

In order to avoid numerical difficulties in calculations, when D becomes very small, we rewrite (16) in the equivalent form

$$\psi_{k+1} = \frac{2\psi_k}{1 + D + \sqrt{(1+D)^2 - 4D\psi_k}}. \tag{17}$$

Equations (13) and (17) constitute the bounded tokamap.

4 Phase Portraits

We first reproduce some typical phase portraits of the *tokamap* [2] and the *revtokamap* [3] using the known expressions for the winding number

$$W(\psi) = \frac{w}{4}(2-\psi)\left(2 - 2\psi + \psi^2\right) \tag{18}$$

for the tokamap and

$$W_R(\psi) = w\left[1 - a(c\psi - 1)^2\right] \tag{19}$$

for the revtokamap. Here

$$a = \frac{w - w_0}{w}, \qquad c = 1 + \left(\frac{w - w_1}{w - w_0}\right)^{1/2} \tag{20}$$

The winding number (18) is a monotonously decreasing function of ψ, while the winding number (19) possesses a maximum which corresponds to a reversed sheer ($s = [\psi/q(\psi)]\, dq(\psi)/d\psi$) configuration.

Some typical phase portraits of these two maps are shown in Figs. 1a and Figs. 2a respectively. It is seen in Fig.1a that trajectories to a significant extent lie outside the physical region $\psi \leq 1$. This tendency increases with increase of the stochasticity parameter K. It can be seen in Fig.2a that even for small values of the stochasticity parameter $K = 2$ and $K = 4$, in revtokamap trajectories leave the physical region. This is related to the fact that $W_R(\psi)$ changes sign when $\psi > 1$.

In Figs. 1b and Figs. 2b we show the corresponding phase portraits of the bounded tokamap and bounded revtokamap.

In bounded tokamap (Fig.1b) we observe that stochastization begins at the physical boundaries, as is clearly seen for $K = 6$. Here two chaotic layers separated by barriers are formed in the vicinity of $\psi = 0$ and $\psi = 1$. It is obvious that the phase portraits of the revtokamap and the bounded revtokamap (Fig.2) are also quite different.

Summarizing we can say that

- The tokamap/revtokamap is a Hamiltonian map, depending on parameter K, under which an initially positive radial coordinate ψ remains always positive, and the polar axis is a barrier that cannot be crossed.

- The bounded tokamap/revtokamap is a Hamiltonian map, depending on parameter K, under which radial coordinate ψ may vary only in the physical range $0 \leq \psi \leq 1$, and that the polar axis $\psi = 0$ and tokamak wall $\psi = 1$ are globally invariant.

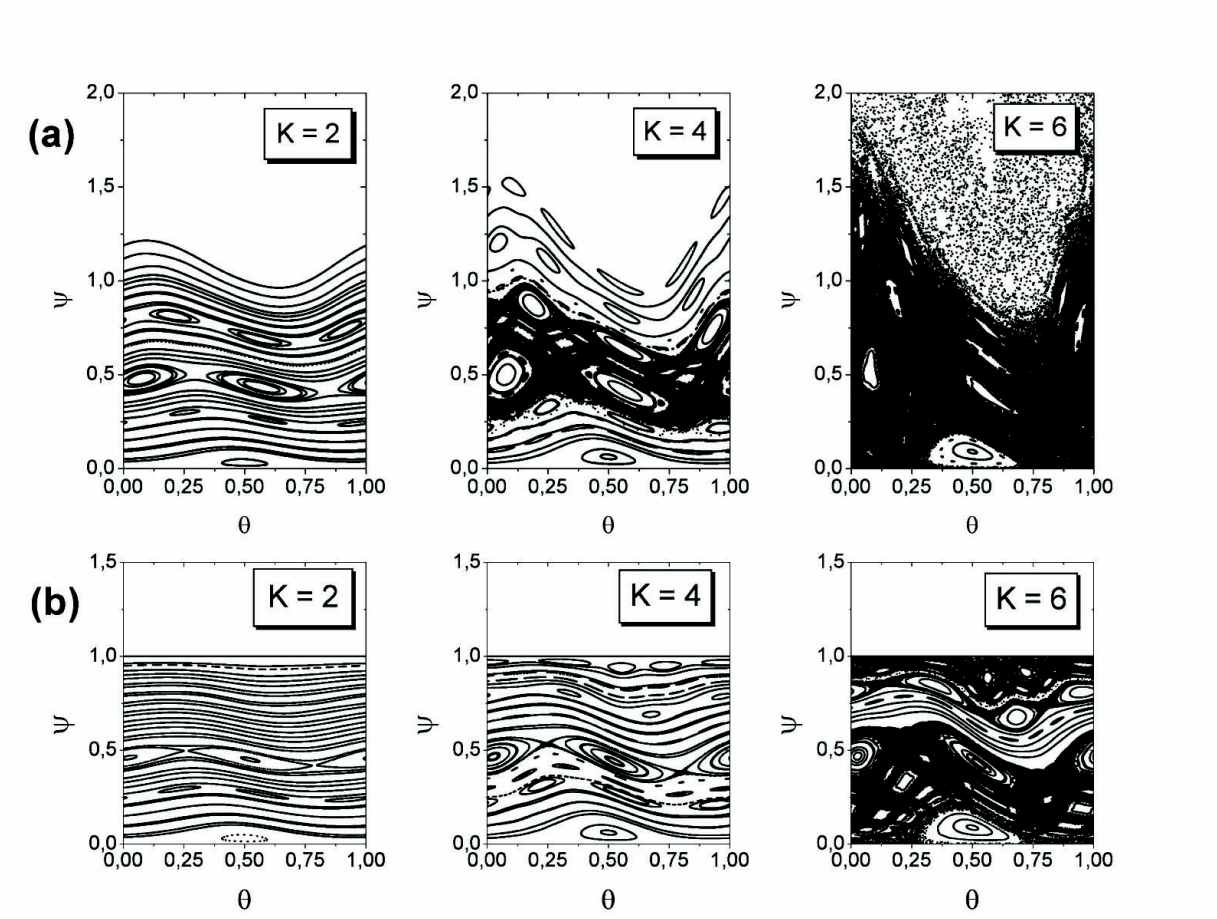

Figure 1: (a) Tokamap and (b) Bounded tokamap regular and chaotic orbits. Here the following initial conditions have been used: twenty points along ψ axis and two points along θ axis. The parameter $w = 1$ in Eq. (18). The number of iterations N=5000.

As next we consider the winding number which is typical for the ASDEX Upgrade tokamak [8]

$$W = \frac{1}{0.8 + 2\psi} \tag{21}$$

In Fig. 3a we show some tokamak phase portraits and in Fig. 3b some bounded tokamak phase portraits obtained with this winding number. It is evident that raising the stochasticity parameter gradually increases stochasticity albeit significantly slower than in the tokamap.

Note, that for the ASDEX Upgrade tokamak the number and nature of fixed points of the tokamap and the bounded tokamap are the same (for details see the Appendix).

It is convenient to discuss differences in the phase portraits of the bounded and unbounded models in terms of Kolmogorov-Arnold-Moser (KAM) barriers.

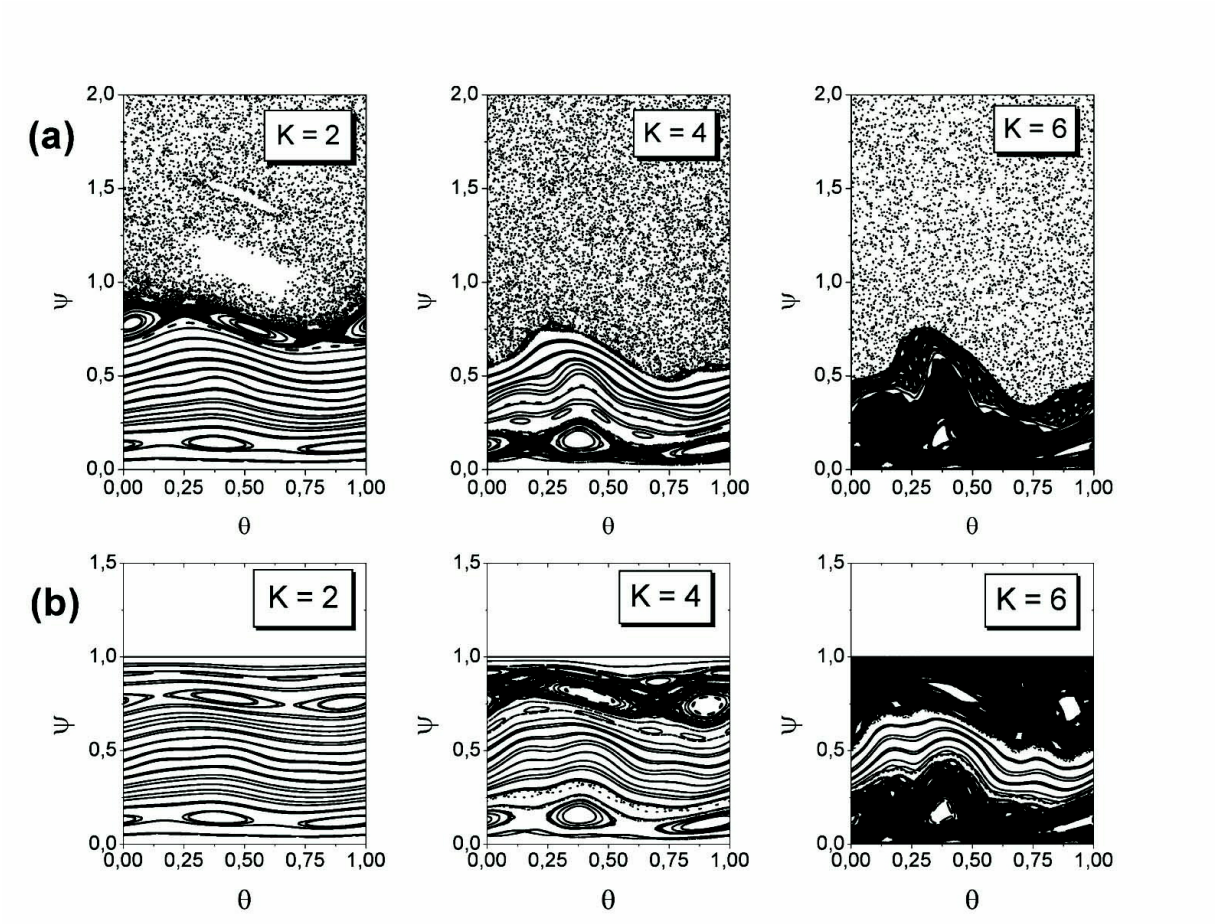

Figure 2: (a) Revtokamap and (b) Bounded revtokamap regular and chaotic orbits. The parameters $w_0 = 1/3$, $w = 2/3$, $w_1 = 1/6$ in Eq. (20). Other conventions as in Fig. 1.

From classical theory of chaos, it is expected that the most resistant KAM tori correspond to surfaces where the safety factor q is equal either to the Golden number or at least to noble numbers defined by a continuous fraction expansion

$$[a_1, a_2, a_3, \ldots, a_j] = a_1 + 1/\left(a_2 + 1/\left(a_3 + 1/\cdots + 1/a_j\right)\right) \tag{22}$$

Here the Golden number has a simple coding:

$$G \equiv 1 + \frac{1}{1+\frac{1}{G}} = \frac{\sqrt{5}+1}{2} = \\ = [1,1,1,1,\ldots 1] = 1.61803399\ldots. \tag{23}$$

It is known that the most robust KAM barrier in the standard map [9] is indeed the one corresponding to safety factor $q = G$, or the winding number $W = 1/G$, which is called the golden KAM.

Solving the cubic equation (18) for the tokamap

$$\frac{1}{G} = \frac{w}{4}(2-\psi)\left(2-2\psi+\psi^2\right) \tag{24}$$

with w=1, we find that the golden KAM is located at $\psi \approx 0.316$. Solving the quadratic equation (19) for the revtokamap

$$\frac{1}{G} = w\left[1 - a\left(c\psi - 1\right)^2\right] \tag{25}$$

we find that there are two golden KAM barriers located at $\psi \approx 0.278$ and $\psi \approx 0.621$, and solving the linear equation (21) for the ASDEX Upgrade

$$\frac{1}{G} = \frac{1}{0.8+2\psi} \tag{26}$$

we find that the golden KAM is located at $\psi \approx 0.409$.

It is evident from Fig. 1a that in the tokamap, the golden KAM is not the most robust KAM barrier [2]. Also in the revtokamap (Fig. 2a), the two golden KAMs are not the most robust KAM barriers. The situation is different in the bounded tokamap, as illustrated in Fig. 4. It can be seen that the Golden KAM at $\psi \approx 0.316$ exists at least up to $K = 4.5$.

The picture is more complicated in the case of the bounded revtokamap, as seen in Fig. 5.

In this case the equation (25) has two roots: $\psi \approx 0.621$ and $\psi \approx 0.278$. It is interesting that the first observed KAM can be attributed to the first root, but the location of the second observed KAM with good accuracy can be described by the equation

$$\frac{5G+2}{8G+3} = w\left[1 - a\left(c\psi - 1\right)^2\right]. \tag{27}$$

Let us now consider the winding number corresponding to ASDEX Upgrade (26). The results are shown in Fig. 6.

It is evident that the golden KAM located at $\psi \approx 0.409$ is present in the tokamap, albeit it is relatively quickly destroyed at $K < 4$, due to the drift of the trajectories to the nonphysical region.

As noted above, it can be said that in the tokamap and revtokamap trajectories systematically drift into unphysical region $\psi > 1$. Such a drift can be regarded as a strong perturbation shifting the most robust KAM surfaces far beyond the physical region, to noble numbers more distant from the golden number G. For example, in [4] the irrational number $[4,2,1,1,...] = 4.382$ has been studied.

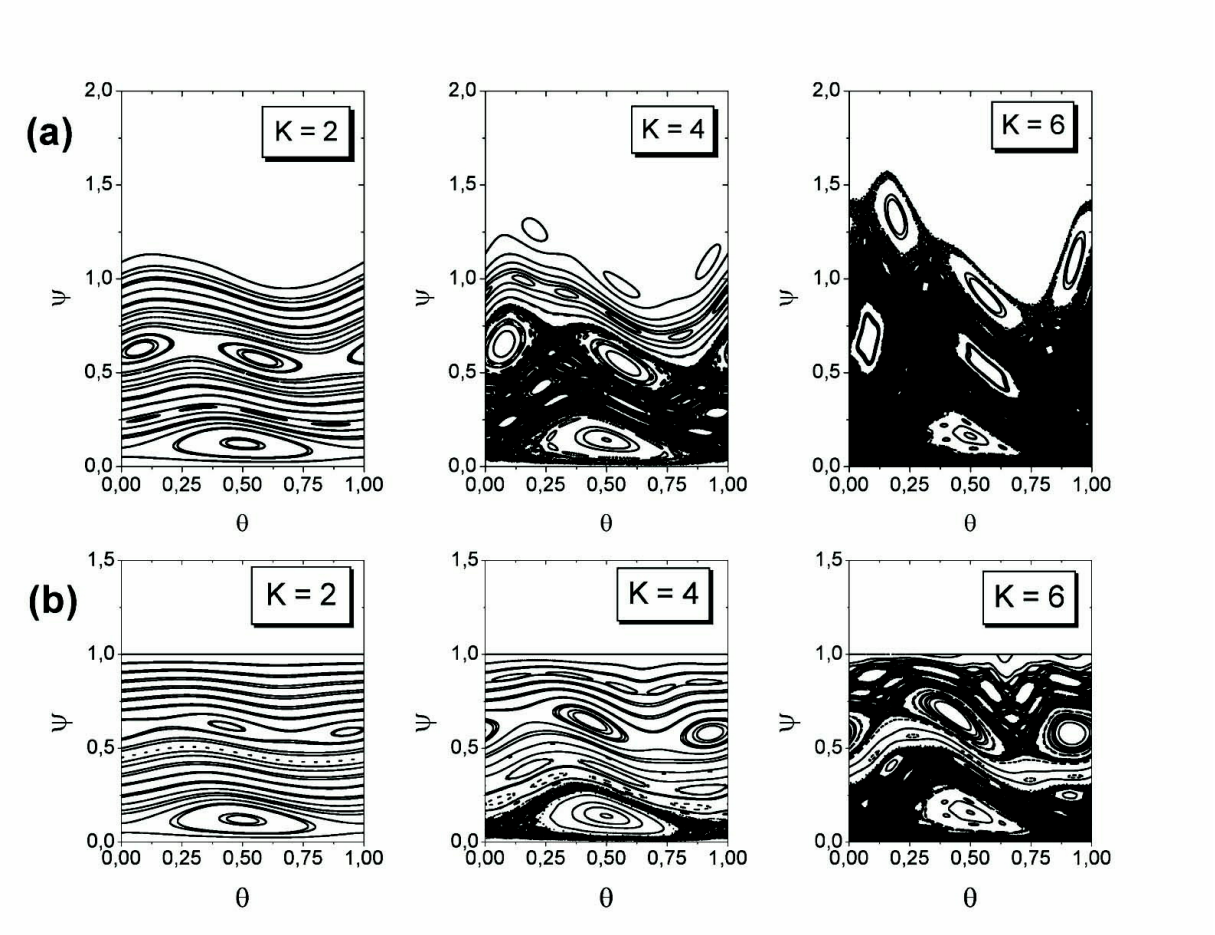

Figure 3: (a) Tokamap and (b) Bounded tokamap phase portrait with Eq. (21).

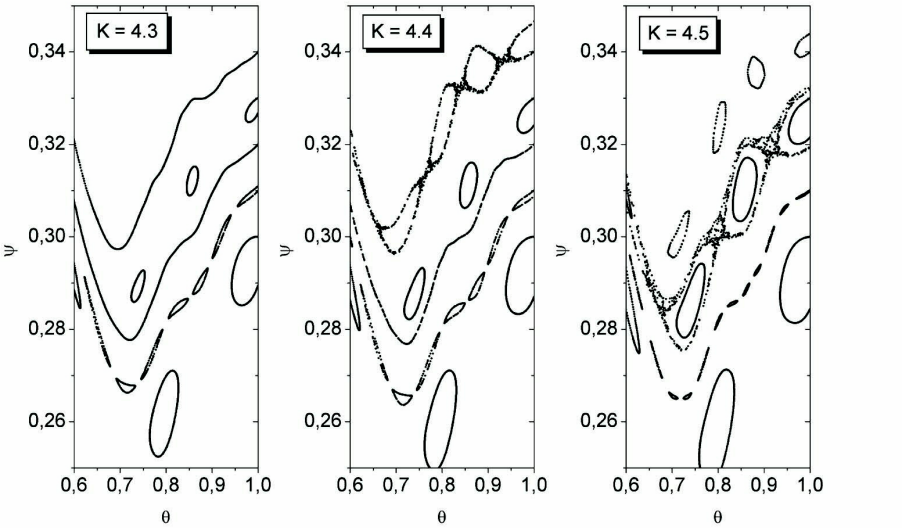

Figure 4: Golden KAM for Bounded tokamap near $W = 1/G$, EQ. (24). Initial conditions: $\theta_0 = 0$ and $\psi_0 = 0.30,\ 0.31,\ 0.32,\ 0.33,\ 0.34$. The number of iterations $N = 10000$.

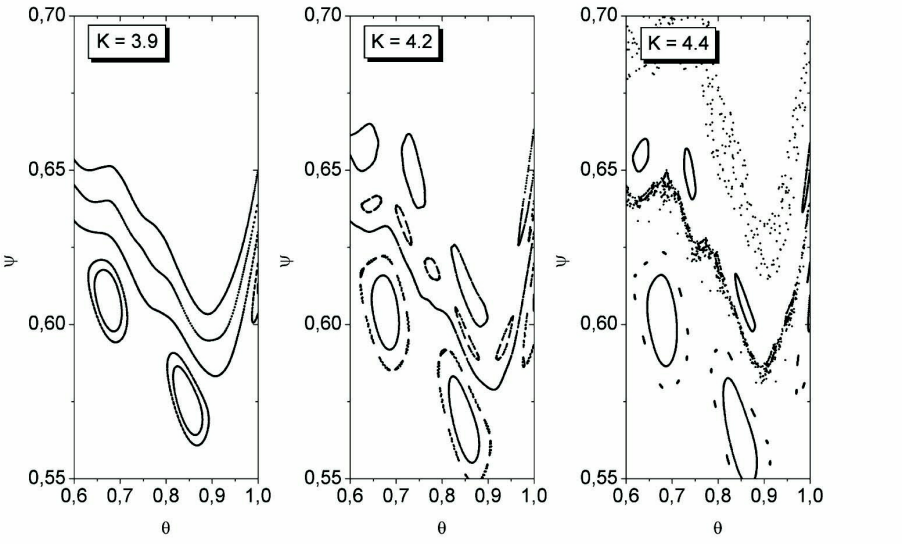

Figure 5: Golden KAM for the bounded revtokamap near $W = 1/G$, Eq. (25). Initial conditions: $\theta_0 = 0$ and $\psi_0 = 0.61,\ 0.62,\ 0.63,\ 0.65,\ 0.66$. The number of iterations $N = 10000$.

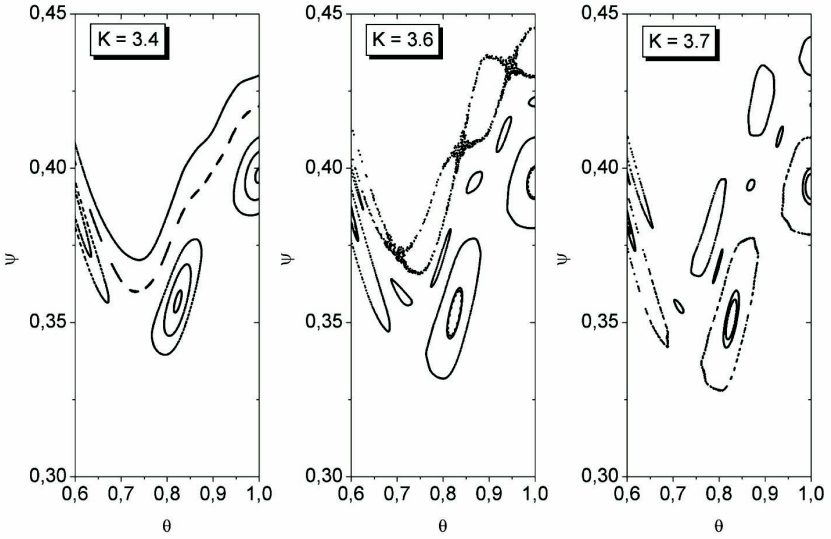

Figure 6: Golden KAM for tokamap near $W = 1/G$, Eq. (26). Initial conditions: $\theta_0 = 0$ and $\psi_0 = 0.39,\ 0.40,\ 0.41,\ 0.42,\ 0.43$. The number of iterations $N = 10000$.

5 Conclusions

We have shown how a simple Hamiltonian map can be constructed in which magnetic field lines are not allowed to cross the plasma boundary. Phase portraits of the new map are quite different comparing with tokamap phase portraits. In particular, we find that in the bounded tokamap the Golden KAM exists up to $K \approx 4$ in contrast to tokamap where the Golden KAM plays no special role. In the case of the winding number (28), considered as an example, the number and the nature of the fixed points of the tokamap and bounded tokamap are the same. The situation may be different for other forms of the winding number. It is obvious that differences in the predictions of the tokamap and bounded tokamap might become significant in those cases when processes at plasma periphery are studied.

6 Acknowledgments

One of us (O.D.) gratefully acknowledges many fruitful discussions with Dr. D. Constantinescu. The authors acknowledge financial support from via fellowships for O.D.

7 Appendix: Fixed Points

We now address the question whether the new form of the function $h(\psi)$ given by Eq. (11) changes the locations of fixed points in the bounded tokamap in comparison with the

tokamap [2]. To be specific, we confine ourselves to the winding number which is typical for ASDEX Upgrade tokamak (27), albeit allowing for a free parameter u

$$W = \frac{1}{u + 2\psi} \tag{28}$$

Fixed points of a mapping are defined as

$$\psi_{k+1} = \psi_k = \psi, \ \theta_{k+1} = \theta_k = \theta. \tag{29}$$

The study of fixed points should be completed by a linear stability analysis. A very simple stability criterion is based on the residue, defined as follows in terms of the trace of the matrix M defining the latter map [10]:

$$R = \frac{1}{4}\left(2 - TrM\right) \tag{30}$$

The fixed point around which the map is linearized is said to be linearly stable whenever $0 \leq R \leq 1$.

It has been found [2] that in the tokamap for $w_m \leq w \leq w_M$, there are two unstable X fixed points on the polar axis: $X_1 = (0, \theta_1)$ and$X_2 = (0, \theta_2)$. Here

$$w_m = 1 - (2\pi)^{-2} K, \tag{31}$$

$$w_M = 1 + (2\pi)^{-2} K. \tag{32}$$

These points are bifurcation points: for $w = w_m$ the fixed points merge at $\theta = 1/2$, and for $w = w_M$ they merge at $\theta = 0$. For w below w_m, or above w_M, the fixed points disappear.

In addition to these fixed points for$w_m \leq w < w_m + 1$, there is exactly one elliptic fixed point $Y_{=}(\psi_1, 1/2)$ within the physical domain, and for $w_M < w < w_M + 1$ there is exactly one hyperbolic fixed point $Y_2 = (\psi_2, 0)$ within the physical domain.

Fixed points of the revtokamap are significantly more complicated. They are listed in Table I of [3].

In order to find fixed points, we substitute Eq. (29) into Eqs. (12) and (13). As a result, we obtain the equations

$$h(\psi)\sin(2\pi\theta) = 0, \tag{33}$$

$$W(\psi) - \frac{K}{(2\pi)^2} h'(\psi)\cos(2\pi\theta) = 0. \tag{34}$$

The resulting residue is given by the expression

$$R = -\frac{K}{4} \cdot \frac{A + \frac{K}{(2\pi)^2} B}{1 + \frac{K}{2\pi} h'(\psi)\sin(2\pi\theta)}, \tag{35}$$

where

$$A = W'(\psi)\, h(\psi)\cos(2\pi\theta), \tag{36}$$

$$B = \left(h'(\psi)\right)^2 \sin^2(2\pi\theta) - h(\psi)\, h''(\psi)\cos^2(2\pi\theta), \tag{37}$$

and $h''(\psi) = -2$.

7.1 Roots of equation $h(\psi) = 0$

There are two roots: $\psi = 0$ and $\psi = 1$. Let us examine first the root $\psi = 0$. Taking into account that $W(0) = w = 1/u$, we obtain the condition

$$G(\theta, K, w, m) \equiv w - \frac{K}{(2\pi)^2}\cos(2\pi\theta) - m = 0, \tag{38}$$

where m is any integer, positive, zero, or negative.

Allowing for the experimental uncertainty in the value of the parameter u in Eq. (28) of the order $0.7 \leq u \leq 1.0$, we obtain a rather narrow interval of allowed w values:

$$0.5 \leq w \leq 1.5. \tag{39}$$

Taking $m = 1$, we reproduce the result obtained in [2]. Equations $G(1/2, K, w_{\min}, 1) = 0$ and $G(0, K, w_{\max}, 1) = 0$ determine the two values:

$$w_{\min} = 1 - \frac{K}{(2\pi)^2}, \tag{40}$$

$$w_{\max} = 1 + \frac{K}{(2\pi)^2}. \tag{41}$$

There are two X fixed points for $w_{\min} \leq w \leq w_{\max}$ and $K \leq 2\pi$, which are unstable, because the corresponding residue is negative

$$R = -\frac{K^2}{4(2\pi)^2}\frac{\sin^2(2\pi\theta)}{1 + \frac{K}{2\pi}\sin(2\pi\theta)}. \tag{42}$$

We now consider the case $\psi = 1$. Substituting this value into Eq. (34) and taking into account that $W(1) = w^* = w/(1 + 2w)$, we obtain the condition

$$S(\theta, K, w, m) \equiv w^* + \frac{K}{(2\pi)^2}\cos(2\pi\theta) - m = 0. \tag{43}$$

It follows from Eq. (39) that the parameter w^* is small and, consequently, Eq. (39) has no physical solutions.

7.2 Roots of equation $\sin(2\pi\theta) = 0$

There are two roots: $\theta = 0$ and $\theta = 1/2$. Let us first consider the root $\theta = 1/2$. Substituting it into Eq. (35), we obtain the equation

$$F_1(\psi, K, w, m) \equiv W(\psi) + \frac{K}{(2\pi)^2}h'(\psi) - m = 0. \tag{44}$$

Examining the behavior of $W(\psi)$ in the interval $0 \leq \psi \leq 1$ and taking into account the fact that $|h'(\psi)| \leq 1$, it is not difficult to notice that only the value $m = 1$ is of interest. The sum $W_+(1) = W(\psi) + \frac{K}{(2\pi)^2}h'(\psi)$ as a function of ψ monotonically decreases from $W_+(0) = w + \frac{K}{(2\pi)^2}$ to $W_+(1) = w^* - \frac{K}{(2\pi)^2}$. Consequently the equation $F_1(\psi_1, K, w, 1) = 0$

has only one root in the physical region, if $w + \frac{K}{(2\pi)^2} > 1$, but $w^* - \frac{K}{(2\pi)^2} < 1$. The second inequality is irrelevant, if we consider $w$values of the order of unity. In other words, for

$$w > w_{\min} = 1 - \frac{K}{(2\pi)^2} \tag{45}$$

there exists the fixed pointY_1.

For $\theta = 1/2$ the residue R can be easily evaluated:

$$R = \frac{K}{4} h(\psi) W'_+(\psi) \tag{46}$$

for $\psi = \psi_1$. It can be readily seen that$R \leq 0$, because $W'(\psi) < 0$ and, hence $W'_+(\psi) < 0$. Thus, the fixed point Y_1 is unstable.

Substituting $\theta = 0$ into Eq. (35), we obtain the equation

$$F_2(\psi, K, w, m) \equiv W(\psi) - \frac{K}{(2\pi)^2} h'(\psi) - m = 0. \tag{47}$$

Taking into account Eq. (39), we consider again only the case $m = 1$. The quantity $W_-(\psi) = W(\psi) - \frac{K}{(2\pi)^2} h'(\psi)$ monotonically decreases as a function of ψ from $W_-(0) = w - \frac{K}{(2\pi)^2}$ to$W_-(1) = w^* + \frac{K}{(2\pi)^2}$. It is evident that the equation $F(\psi_2, K, w, 1) = 0$ has only one root, if $w - \frac{K}{(2\pi)^2} > 1$, but $w^* + \frac{K}{(2\pi)^2} < 1$. The second inequality again is irrelevant. For

$$w > w_{\max} = 1 + \frac{K}{(2\pi)^2} \tag{48}$$

we obtain the fixed point Y_2 with the corresponding residue

$$R = -\frac{K}{4} h(\psi) W'_-(\psi). \tag{49}$$

Here the sign of the function $W'_-(\psi)$ is not fixed. However, if the root ψ_2 of the equation $W_-(\psi_2) = 1$ is used and the conditions are searched for which $R = 0$, $W'_-(\psi_2) = 0$, one can easily show that there are no roots when the bounds (39) are imposed. In other words, the inequality $W'_-(\psi_2) < 0$ holds, which means that the fixed point Y_2 is stable.

The conclusion can be drawn that with imposed bounds (39) characteristic for the ASDEX Upgrade tokamak the number and nature of fixed points of the tokamap and the bounded tokamap are the same. This means that the physical upper limit (10) does not generate any new fixed points. This is related to the fact that the function (28) is monotonous. The situation is different in the case of the revtokamap, where the function (25) has a local maximum.

References

[1] S.S. Abdullaev, Construction of Mappings for Hamiltonian Systems and Their Applications (Springer, Berlin, 2006).

[2] R. Balescu, M. Vlad, and F. Spineanu, Phys. Rev. E 58, 951 (1998).

[3] R. Balescu, Phys. Rev. E 58, 3781 (1998).

[4] J.H. Misguich, J.-D. Reuss, D. Constantinescu, G. Steinbrecher, M. Vlad, F. Spineanu, B. Weyssow, and R. Balescu, Ann.Phys. Fr. 28, 1 (2003).

[5] S.S. Abdullaev, K.H. Finken, and K.H. Spatschek, Phys. Plasmas 6, 153 (1999).

[6] I. Pavlenko, B. Rapoport, B. Weyssow, and D. Carati, Phys. Plasmas 10, 1083 (2003).

[7] A. Wingen, K.H. Spatschek, and S. Abdullaev, Contrib. Plasma Phys. 45, 500 (2005).

[8] S. Guenter, C. Angioni, M. Apostoliceanu et al, Nucl. Fusion 45, S98 (2005).

[9] B. Chirikov, Phys. Rep. 52, 265 (1979).

[10] J.M. Greene, J. Math. Phys. 20, 1183 (1979).